

The role of exposed silver in CO oxidation over MgO(001)/Ag(001) thin films

Franziska Ringleb, Yuichi Fujimori, Matthew A. Brown[#], William E. Kaden, Florencia Calaza, Helmut Kuhlenbeck, Martin Sterrer*, Hans-Joachim Freund

Department of Chemical Physics, Fritz-Haber-Institut der Max-Planck-Gesellschaft, Faradayweg 4-6, 14195 Berlin, Germany

[#] present address: Institute for Chemical and Bioengineering, ETH Zürich, Switzerland.

* corresponding author. E-mail: sterrer@fhi-berlin.mpg.de

Abstract

The reactivity of MgO(001) films deposited on Ag(001) and Mo(001) in CO oxidation as a function of oxide film thickness was investigated experimentally at ambient pressure reaction conditions. MgO films grown on Mo(001) were found to be inactive in CO oxidation, whereas activity enhancement with decreasing oxide film thickness was observed for MgO(001)/Ag(001). In-situ infrared and post-reaction X-ray photoemission data showed that ultra-thin MgO films interact much more strongly with the reactants and residual water than bulk-like MgO. Poisoning of the MgO surfaces by the resultant accumulation of carbonate and hydroxyl species is suggested to inhibit the reactivity in CO oxidation. Detailed investigations of the surface structure of MgO(001)/Ag(001) films indicate that silver ad-islands on Ag(001), which are formed during MgO growth, are responsible for the enhancement of CO oxidation activity over ultrathin MgO(001)/Ag(001) films.

Keywords: Ultrathin films, Oxide surfaces, Reactivity, CO oxidation, Charge transfer.

1 Introduction

Metal oxide films grown on single-crystal metal substrates are well-accepted model systems in fundamental heterogeneous catalysis research [1-4]. In a thickness regime where their electronic and structural properties resemble that of the corresponding bulk material, they represent suitable model supports for deposited metal clusters and particles, and allow the properties of the substrate, metal particles and adsorbates to be studied in detail using standard methods of surface science. On the other hand, oxide islands grown on metal substrates (inverse catalysts) have been used for studying the specific effect of metal/oxide boundary sites in catalysis [5-7]. Ultrathin oxide films range in-between these two extremes being films of only a few monolayers (ML) thickness that completely cover the metal substrate. For those ultra-thin films that are only weakly coupled to the metal substrate, the presence of the nearby metal/oxide interface is expected to not perturb the properties of the film surface. However, strongly coupled (e.g. due to hybridization of metal and oxygen states) metal/oxide systems may give rise to unexpected physical and electronic properties [8], which are of potential interest for catalysis [9].

Magnesium oxide (MgO) thin films grown on Mo(001)[10] and Ag(001)[11] have been the subject of active research over the past 20 years. In particular, the film-thickness dependent properties of these films have recently come under scrutiny. Early on it has been realized that Ag(001)-MgO boundary sites are highly reactive and capable of dissociating water even in ultrahigh vacuum (UHV) environment [12,13]. In 2001, Schintke et al. demonstrated that MgO(001) films grown on Ag(001) exhibit bulk-like properties (e.g. a bulk-like band-gap) when the MgO film-thickness is 3 monolayers (ML) [14]. However, Pacchioni and coworkers have later shown that adsorbates on thin MgO films of 2-3 ML thickness might experience an influence of the metal substrate underneath the oxide [15]. According to theoretical predictions, the reduction of the metals' work function by the deposited MgO film in combination with adsorbates exhibiting a high electron affinity (e.g. Au atoms or Au clusters) results in charge transfer from the metal to the substrate and stabilization of the charged adsorbate by polaronic distortion within the oxide film and the formation of an image charge within the metal substrate [15-17]. Scanning tunneling microscopy (STM) studies have later confirmed the theoretical predictions [18-22].

Charge transfer from the metal substrate through the oxide thin film into an adsorbate may be of importance in the activation of molecules for catalytic reactions. As shown in the

computational study of Zhang et al., activation of O₂ molecules at the boundary sites of MgO thin film-supported Au clusters leads to a significant lowering of the barrier for CO oxidation [23]. Along the same lines, Hellman et al. proposed that CO oxidation on metal-supported MgO thin films, where adsorbed oxygen molecules are stabilized as superoxide anions, proceeds with lower activation barrier than on metal surfaces [24]. Experimental evidence for the activation of molecular oxygen on MgO thin films was later provided in an electron spin resonance investigation, where superoxide anions (O₂⁻) were observed to spontaneously form on 4 ML MgO(001)/Mo(001) upon O₂ adsorption at low temperature [25].

While much of the initial interest in the particular properties of thin oxide films was focused on MgO thin film systems, an experimental demonstration verifying the proposed promotional effect of charge transfer through oxide films in catalytic reactions has been presented for 1 ML FeO(111) films grown on Pt(111). Under oxygen-rich CO oxidation reaction conditions, FeO(111)/Pt(111) was reported to be at least 5 times more active in low-temperature CO oxidation than the Pt(111) substrate [26]. The active phase in this catalytic system was found to be an O-Fe-O sandwich layer, which forms by activation of adsorbed oxygen via charge transfer from the metal substrate and subsequent dissociation and incorporation of oxygen into the FeO lattice under high oxygen chemical potentials [27]. While several other oxide/metal combinations have meanwhile been tested for enhanced catalytic activity in CO oxidation [28], experimental verification of the promotional effect of a metal support in CO oxidation over ultra-thin MgO films is still lacking.

In this study, we examined the activity of thin MgO films grown on Ag(001) and Mo(001) as well as of the bare metal substrates in CO oxidation at ambient pressure reaction conditions. Our results show that Mo(001) and MgO thin films grown on Mo(001) are inactive in CO oxidation under the reaction conditions applied in this study. An enhancement of CO oxidation activity with decreasing MgO film thickness is seen for films deposited on Ag(001). Our investigation of the growth mode of MgO films on Ag(001) and post-reaction surface characterization shows how careful one has to be not to jump to conclusions without a detailed knowledge of the surface properties of these samples.

2 Experimental section

The experiments were carried out within a UHV chamber system consisting of a preparation/analysis chamber equipped with standard tools for single-crystal and thin film

preparation, a low-energy electron diffraction (LEED) apparatus, a quadrupole mass spectrometer for temperature programmed desorption (TPD) experiments, and a dual-anode X-ray source and a hemispherical electron analyzer for X-ray photoelectron spectroscopy (XPS). An UHV-elevated pressure cell connected to the bottom of the main UHV chamber, which is equipped with CaF₂ windows for optical access of the sample to infrared radiation, allows to record in-situ infrared reflection absorption (IRA) spectra at up to 1 bar total pressure. The single-crystal samples were mounted on a manipulator, which served to transfer the sample between the preparation chamber and the elevated pressure cell. The samples could be heated in UHV up to 1400 K via resistive heating, or cooled to 90 K using liquid nitrogen.

MgO thin film preparation. The double-side polished Ag(001) and Mo(001) disks used as substrates were cleaned by repeated sputter/anneal cycles. The Mo(001) crystal was additionally oxidized to remove carbon residues from the surface. The long-range order and cleanliness of the samples were verified with LEED and XPS. MgO(001) thin films of various thickness were grown on the metal single-crystal substrates by reactive deposition of Mg in a 1×10^{-6} mbar oxygen background and at a substrate temperature of 573 K. The deposited amount of Mg was calibrated using a quartz micro-balance.

Reactivity studies. We examined the reactivity of MgO(001) thin films grown on Ag(001) and Mo(001) as well as of the bare metal single-crystal substrates in the CO oxidation reaction at elevated pressure in a stoichiometric (CO:O₂ = 2:1) reaction mixture within the UHV-elevated pressure cell. Typically, the freshly prepared samples were pre-annealed at 673 K in UHV in the elevated pressure cell and a background IR spectrum was recorded after cool-down to room temperature (RT). The reaction gases (5 mbar CO and 2.5 mbar O₂, balanced by He to 1000 mbar total pressure) were then introduced at RT and IRA spectra were taken at defined intervals during heating the sample from RT to 423 K at a constant heating rate of 1 K/min. During the reaction, the gas mixture was mixed with a gas circulation pump. The integrated area of the gas-phase IR absorption signal of CO₂ evolving during the CO oxidation experiments was taken as a measure for the catalytic activity of the samples.

Additional characterization. Additional surface characterization of MgO(001)/Ag(001) thin film samples was carried out in separate UHV chambers: Low-energy ion scattering (LEIS) experiments were carried out within a chamber housing a hemispherical electron analyzer and an ion gun ($E_{\text{prim}}(\text{He}^+) = 1 \text{ keV}$). A home-built low-temperature scanning tunneling microscope (STM) operated at liquid He temperature was used for morphological characterization of MgO(001)/Ag(001) ultrathin films. Surface sensitive photoemission data

from the films were obtained at the synchrotron radiation facility (beamline UE52) of Helmholtz-Zentrum, Berlin.

3 Results and Discussion

3.1 Catalytic tests

CO oxidation over bare Ag(001) and Mo(001) surfaces

Prior to studying thin metal-supported MgO films, the bare metal single-crystal surfaces used as substrates for MgO film growth have been examined with respect to their activity in CO oxidation. In Figure 1a we present an IRA spectrum taken at 300 K from Ag(001) after introduction of the reaction mixture (5 mbar CO, 2.5 mbar O₂, balanced by He to 1000 mbar total pressure) (dotted line), which is dominated by the gas-phase absorption of CO centered at 2143 cm⁻¹. After heating the Ag(001) crystal in the reaction environment to 423 K, a second absorption signal at 2350 cm⁻¹ typical of gas-phase CO₂ has evolved (see red curve in Figure 1a), indicating CO oxidation activity of Ag(001). Silver is known to be active in selective oxidation reactions and the contribution of different surface and subsurface oxygen species to the catalytic activity has been studied in detail in the past [29,30]. Post-reaction XPS analysis of our Ag(001) sample indeed provided some evidence for the presence of oxygen (Figure 1c) and a corresponding small contribution of Ag^{δ+} species on the Ag(001) surface (Figure 1b). According to previous studies, the main O 1s species observed in this work, which exhibits a binding energy (BE) of 530.3 eV, is assigned to electrophilic oxygen (Oα₃ in Ref. [29]), while the smaller contribution with a O 1s BE of 529.3 eV falls within the BE range reported for oxide-like species at steps (Oα₂ in Ref. [29]).

In contrast to Ag(001), the Mo(001) substrate is completely inactive under the experimental conditions applied, as indicated by the lack of a CO₂ gas-phase signal in the corresponding IRA spectra (Figure 1d). The post-reaction XPS analysis indicates that the Mo(001) surface becomes oxidized during exposure to the reaction mixture. In comparison to the clean Mo(001) substrate, which gives rise to a single Mo 3d doublet exhibiting a Mo 3d_{5/2} BE of 228.0 eV, which corresponds to metallic Mo, the Mo 3d spectrum of the reacted sample consists of three individual Mo 3d doublets with 3d_{5/2} BE's of 228.0 eV (Mo⁰), 229.4 eV (Mo⁴⁺) and 232.2 eV (Mo⁶⁺), respectively (Figure 1e) [31,32]. The presence of contributions in the O 1s region (Figure 1f) supports the conclusion that the surface of the Mo substrate

becomes oxidized in the presence of the reaction mixture. CO oxidation over Mo-oxides proceed via a Mars-van-Krevelen mechanism, according to which surface oxygen species are converted by CO to CO₂ and the vacant oxygen sites are replenished by dissociative adsorption of molecular oxygen. The activation energy of the catalytic CO oxidation over Mo-oxides is high and significant turn-over is observed only if the reaction temperature exceeds 600 K [33,34]. Because of experimental limitations, the samples used in the present study could not be heated above 423 K in the presence of the reaction mixture. This explains the observed lack of CO oxidation activity.

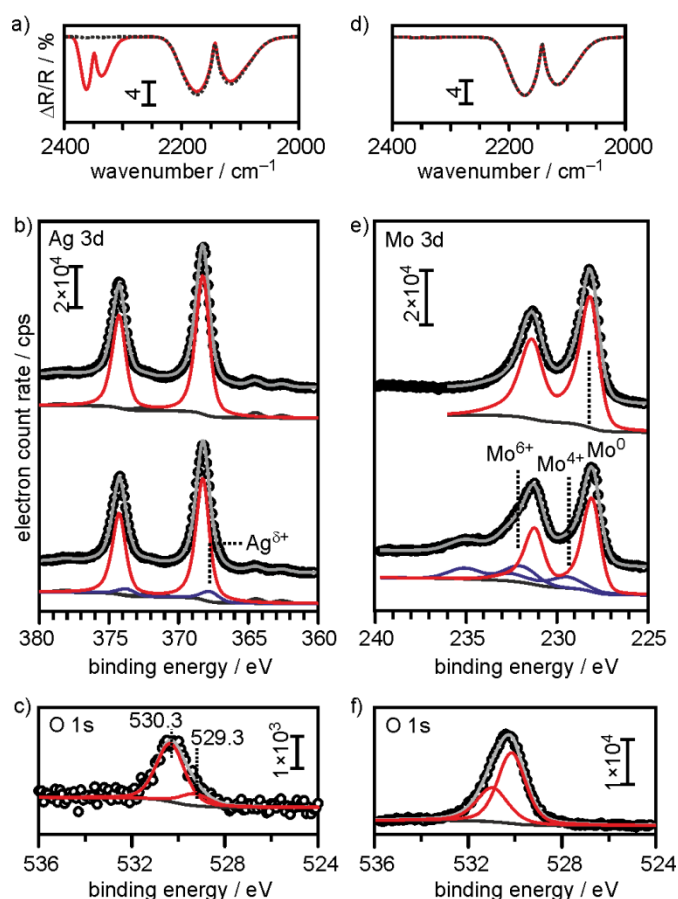


Figure 1. a) IRA spectra taken from Ag(001) in the presence of the reaction mixture (5mbar CO, 2.5 mbar O₂, balanced to 1000 mbar by He) at room temperature (dotted black line) and at 423 K (solid red line). b) Ag 3d photoemission spectra (circles) and results of fits to the spectra (solid lines) for clean Ag(001) (top) and taken after exposure to CO oxidation conditions (bottom). c) O 1s photoemission spectrum of Ag(001) taken after exposure to CO oxidation conditions. d-f) are similar to a)-c), but for Mo(001).

CO oxidation over metal-supported MgO films

The amount of gas-phase CO₂ evolved during heating Ag(001) and MgO(001)/Ag(001) films of different thickness (from 2 ML MgO to 50 ML MgO) in the presence of the CO/O₂ mixture is presented in Figure 2a. We note the similar thermal behavior of the various samples with onset of CO₂ production at 350 K. The results are summarized in Figure 2b, where we plot the total amount of CO₂ produced during the reaction as a function of the MgO film thickness. Among the samples studied, the bare Ag(001) surface exhibited the highest activity in CO oxidation, followed by the 2 ML and 5 ML thin MgO(001)/Ag(001) films. The 10 ML and 50 ML MgO(001)/Ag(001) films exhibited the lowest, albeit similar, CO oxidation activity. For comparison, we show in Figure 2c the activity results for MgO(001)/Mo(001) thin films. In contrast to MgO(001)/Ag(001), both the ultra-thin (3 ML) and the thick (30 ML) MgO film samples were essentially inactive in CO oxidation (note the different scaling of the ordinates in Figure 2b and Figure 2c).

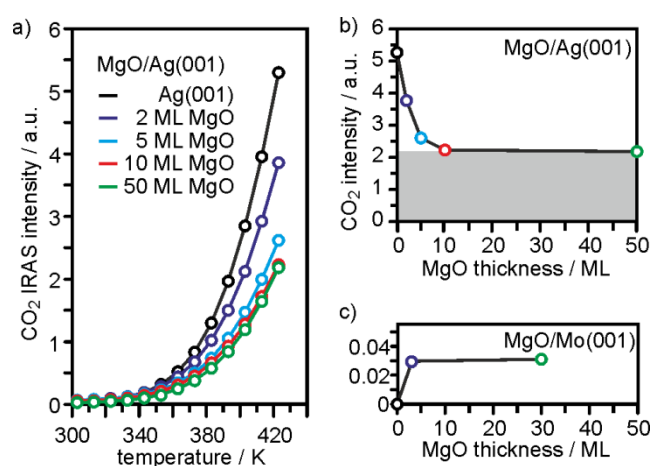


Figure 2. a) Evolution of CO₂ (displayed as integrated intensity of the CO₂ gas-phase IR absorption) during CO oxidation conditions (5 mbar CO, 2.5 mbar O₂) as a function of heating temperature for Ag(001) and MgO(001)/Ag(001) thin film samples of different MgO film thickness. b) Summary of the MgO film thickness-dependent CO oxidation activity (integrated CO₂ gas-phase absorption at 423 K) for MgO thin films grown on Ag(001). c) Summary of the MgO film thickness-dependent CO oxidation activity for MgO thin films grown on Mo(001).

An explanation for the constant CO oxidation activity observed for thick (10 ML and 50 ML) MgO(001) films on Ag(001) can be provided by considering the sample geometry of the Ag(001) single-crystal used in this study. It is a disc-shaped sample with a diameter of 10 mm and a thickness of 2 mm. MgO films were grown on the polished top and bottom plane of the disc, while its lateral surface, which contributes about 30 % to the total surface area, cannot be

covered by MgO and remained largely bare Ag. Taking into account that the lateral surface is non-polished and exhibits a high degree of roughness and defectiveness, it is easily conceivable that its contribution to the overall CO oxidation activity of the Ag(001) sample is 40 % (grey shaded area in Figure 2b). The presence of bare Ag on the lateral surface can, however, not explain the increased CO oxidation activity of ultra-thin (< 10 ML) MgO(001)/Ag(001) films, since its contribution does not depend on the thickness of the films.

It would be tempting to attribute the observed activity enhancement for ultra-thin MgO films grown on Ag(001) compared to thick films to the film thickness-dependent activation of oxygen as proposed in computational studies [24]. However, since Ag(001) is the most active catalyst among the samples studied in this work, and MgO films grown on Mo(001) are shown to be completely inactive in CO oxidation, alternative explanations for the experimental observations need to be considered as well. In particular, the possible role of reaction site poisoning due to a strong interaction of the reactants with the surfaces under elevated pressure conditions and the influence of surface irregularities introduced during MgO film growth need to be carefully examined. In the following sections we present results of a detailed surface characterization study of MgO(001)/Ag(001) thin films, which suggest that these additional parameters strongly influence the reactivity of MgO thin-film samples.

3.2 Poisoning

As demonstrated recently, superoxide anions, which represent the activated form of molecular oxygen in the computationally proposed CO oxidation mechanism over thin MgO films, spontaneously form on 4 ML MgO(001)/Mo(001) surfaces upon adsorption of O₂ at low temperature under UHV conditions [25]. According to computational results, the activation barrier for the reaction of the superoxide intermediate with CO on regular MgO(001) terrace sites is small (0.3 eV), and the formation and subsequent release of CO₂ is energetically preferred over carbonate formation [24]. Real MgO thin film surfaces exhibit in addition to regular terraces a number of defect sites such as low-coordinated step, kink, and corner sites (as well as MgO-Ag interface sites), where carbonate may more easily be formed or stabilized and thus lead to reaction site poisoning. In addition, thin MgO(001)/Ag(001) films are highly reactive towards water and become hydroxylated even under UHV conditions through interaction with residual water molecules in the chamber [12].

Evidence for carbonate and hydroxyl contamination of the MgO(001)/Ag(001) films used in our experiments comes from IRAS and XPS data. As shown in Figure 3a, where we present IRA spectra taken from MgO(001)/Ag(001) thin film samples after admission of the reaction mixture at room temperature (black curves) and at 423 K during the reaction (red curves), vibrational bands appear at $\sim 1390\text{--}1420\text{ cm}^{-1}$ and 1223 cm^{-1} , which are assigned to the symmetric OCO stretch and the COH bending modes of bicarbonate species, respectively. This assignment is supported by the simultaneous appearance of an OH vibration at 3629 cm^{-1} (data not shown). A clear preference for the formation of bicarbonate on the thinner MgO(001)/Ag(001) films is evident based on the observed IR intensities. While this surface species is stable throughout the reaction on thick films (10 ML and 50 ML MgO), a partial (5 ML MgO) or complete (2 ML MgO) transformation into a carbonate species characterized by a vibrational mode at 1565 cm^{-1} is observed on the thinner films.

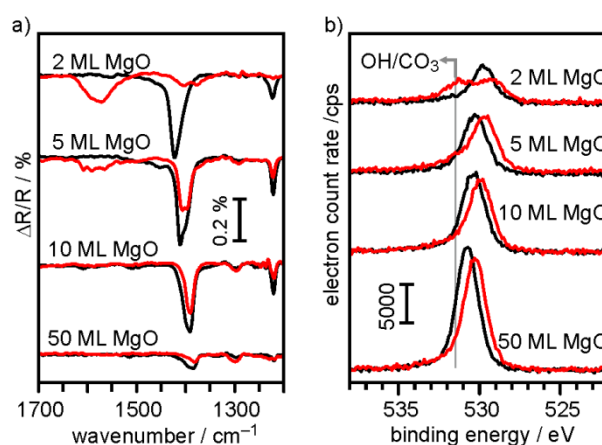


Figure 3. a) IRA spectra of MgO(001)/Ag(001) thin films of different thickness taken after admission of the reaction mixture (5 mbar CO, 2.5 mbar O₂, balance by He to 1000 mbar) at room temperature (black curves), and during CO oxidation reaction at 423 K (red curves). b) O 1s photoemission spectra of clean MgO(001)/Ag(001) thin films of different thickness (black curves) and of the same films after CO oxidation reaction (red curves).

Formation of bicarbonate species requires the simultaneous presence of CO, O₂ and water or hydroxyls on the surface of the films. The O 1s XPS data displayed in Figure 3b show that the surfaces of pristine MgO films are essentially free of hydroxyls in UHV (black curves; only one O 1s signal around 530 eV, which is assigned to the oxide anions of MgO, is observed irrespective of film thickness; the shift of the O 1s peak to higher binding energy with increasing film thickness has been observed and described previously [35]). In the post-reaction O 1s XP spectra (Figure 3b, red curves), in particular of the ultrathin films, significant spectral changes are seen compared to the corresponding clean state, which point

to a chemical modification of the films' surfaces during the reaction. In the case of the 2 ML MgO(001)/Ag(001) thin-film sample, a second O 1s signal with a binding energy of 531.7 eV, which consists of O 1s contributions from carbonates and hydroxyls, can be clearly detected. This signal is present as a shoulder on the high binding-energy tail of the main O 1s signal of 5 ML MgO(001)/Ag(001), but is hardly discernible in the spectra of the thicker films, resembling the different reactivity of ultra-thin and thick MgO films. Although particular care was taken to dose the reaction gases into the reaction cell as clean as possible, water contamination of the MgO film surfaces could not be completely avoided under reaction conditions. Obviously, minuscule amounts of residual water adsorbed on the walls of the UHV chamber, which are released into the gas-phase upon filling the reaction cell with the reactant gases, and the high reactivity of ultra-thin MgO films toward water dissociation are responsible for the build-up of hydroxyl contamination.

Together, the IRAS and XPS data presented in Figure 3 show that ultra-thin MgO(001)/Ag(001) films are significantly more reactive than bulk-like MgO, which makes their surfaces highly susceptible for surface poisoning in the reaction gas environment. This applies also to ultra-thin MgO(001)/Mo(001) samples, where qualitatively similar results have been obtained (not shown). We suggest that in our experiments poisoning is the main reason for the lack of reactivity of ultra-thin MgO films in CO oxidation according to the reaction mechanism proposed computationally, and that the enhancement of CO oxidation activity observed for ultra-thin MgO(001)/Ag(001) films (Figure 2b) must be attributable to a different mechanism. Next, we provide evidence that MgO(001)/Ag(001) thin films expose a significant amount of Ag, which most likely accounts for the observed activity enhancement.

3.3 Evidence for exposed Ag on MgO(001)/Ag(001) thin film samples

We investigated MgO(001)/Ag(001) films with surface-sensitive methods that allow us to directly probe the Ag surface contribution and to quantify the amount of Ag on the surface of MgO films of different thickness. Low-energy ion scattering (LEIS) is perfectly suited for this purpose because it allows the elemental composition of exclusively the outermost atomic layer of the samples to be determined. In Figure 4a, we present LEIS spectra taken from the clean Ag(001) surface as well as from MgO(001)/Ag(001) samples with a nominal MgO film thickness ranging between 1.5 ML and 25 ML. Intensity of scattered He ions is observed from the individual samples at normalized energy losses of $E/E_0 = 0.84$, 0.54 and 0.40, which, taking the scattering geometry into account and with $E_0 = 1$ keV used in this study, can be

attributed to He ion scattering from Ag, Mg and O, respectively. The results show that, except for clean Ag(001), the Mg and O contributions scatter only slightly around a constant value, which is expected for surfaces that are mainly terminated by MgO. For a perfect layer-by-layer MgO film growth, the Ag contribution would be expected to disappear along with completion of the first monolayer of MgO. By contrast, we find a steady attenuation of the Ag surface contribution with increasing MgO film thickness. In fact, the Ag signal is clearly detectable on MgO films with a thickness of up to 10 ML, and disappears only for the thickest film investigated in this study (25 ML MgO).

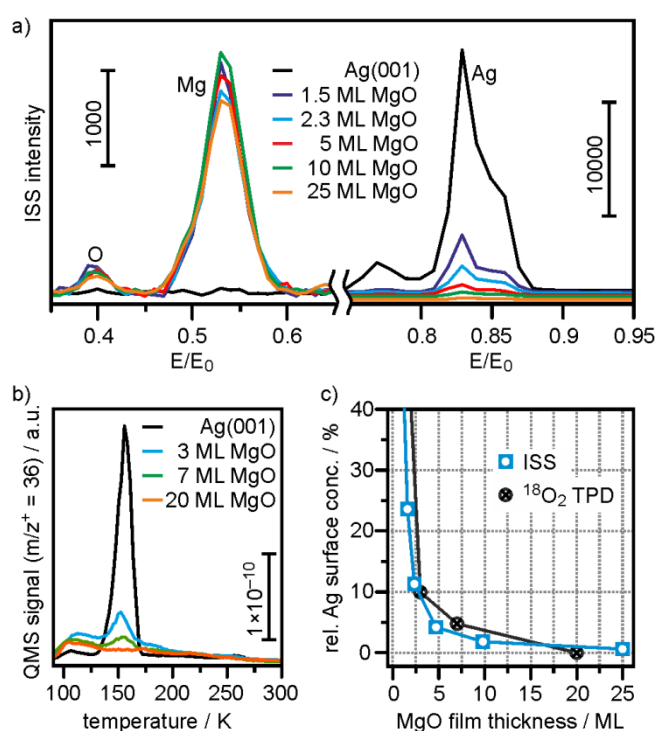


Figure 4. a) Low-energy ion scattering spectra of Ag(001) and MgO(001)/Ag(001) thin films of different MgO film thickness. b) $^{18}\text{O}_2$ ($m/z^+ = 36$) desorption from Ag(001) and MgO(001)/Ag(001) thin films of different MgO film thickness during a temperature-programmed desorption experiment following a saturation coverage of $^{18}\text{O}_2$ at 90 K. c) Relative area of exposed Ag (referenced to clean Ag(001)) on MgO(001)/Ag(001) films as a function of the MgO film thickness calculated from the data presented in a) and b).

To confirm the results of the LEIS experiments, we studied the adsorption of molecular oxygen, which forms a stable, chemisorbed molecular adsorbate on Ag(001) below 150 K [36]. Figure 4b shows the results of temperature-programmed desorption (TPD) experiments following adsorption of a saturation dose of $^{18}\text{O}_2$ at 100 K on Ag(001) and MgO(001)/Ag(001) samples with a nominal MgO film thickness of 3 ML, 7 ML and 20 ML, respectively. In agreement with previous studies, $^{18}\text{O}_2$ desorbs from the clean Ag(001) surface

at 150 K [37]. As expected from the results of and in accordance with the LEIS data clear $^{18}\text{O}_2$ desorption signals, although attenuated, are detected also from the MgO(001)/Ag(001) samples exhibiting a nominal MgO film thickness of 3 ML and 7 ML. The adsorption of oxygen is completely blocked in the case of 20 ML MgO(001)/Ag(001) as indicated by the lack of the sharp desorption peak at 150 K for this sample. Increasing background $^{18}\text{O}_2$ desorption from all MgO(001)/Ag(001) samples is observed in the temperature interval between 100 K and 200 K, which most likely originates from $^{18}\text{O}_2$ adsorption at defect sites of the MgO surface.

The results of the LEIS and $^{18}\text{O}_2$ -TPD experiments are summarized in Figure 4c. This plot displays the area of exposed Ag on the MgO thin film samples, relative to that of the clean Ag(001) surface, as a function of the nominal MgO film thickness. (The various contributions were determined from the integrated peak areas of the corresponding Ag-LEIS and $^{18}\text{O}_2$ -TPD signals). There is overall very good agreement between the two independent methods of analysis with respect to the concentration of Ag on the surface of the samples. The data clearly shows that a considerable fraction of the surface of MgO(001)/Ag(001) samples with a nominal MgO thickness below 10 ML consists of exposed Ag, and that the amount of deposited MgO must exceed a nominal coverage of 20 ML in order to ensure complete covering of the Ag substrate.

3.4 Nature of exposed Ag on MgO(001)/Ag(001) samples

While the experiments reported in the previous section give strong evidence of the presence of exposed Ag on MgO(001)/Ag(001) thin films, the results do not provide a conclusion about the nature of exposed Ag on these samples. Several possibilities exist, including (i) incomplete coverage of the Ag(001) substrate by the MgO film, (ii) nucleation of Ag ad-particles on the surface of the MgO films, (iii) embedding of Ag atoms or Ag particles in the MgO film, or (iv) growth of Ag ad-islands of several nanometer height on the Ag(001) surface during MgO film growth. In order to shed more light on this aspect, we re-examined the morphology of MgO grown on Ag(001) with scanning tunneling microscopy (STM).

STM images of MgO monolayer-islands formed by deposition of ~ 0.5 ML MgO on Ag(001) are presented in Figure 5a. The two images were recorded from the same area of the sample, but with different bias voltage: + 3 V (top) and + 1 V (bottom). MgO islands appear with enhanced contrast at the more positive sample bias (Figure 5a, top) due to tunneling through the empty conduction band states of MgO. The MgO islands are square-shaped and regularly distributed over the Ag(001) surface, in agreement with previous studies [38-40]. At a bias

voltage of + 1 V the tunneling probability through MgO is significantly reduced and the morphology of the Ag(001) surface underneath becomes more apparent (Figure 5a, bottom). These images reveal a strong modification of the Ag(001) surface upon MgO deposition: Regular, straight Ag(001) steps are hardly observed and MgO islands near steps appear to be embedded in the Ag layer. As noted in Ref. [38], Ag ad-atom diffusion at the elevated substrate temperature employed during MgO film growth is responsible for the observed morphological changes of the Ag(001) surface.

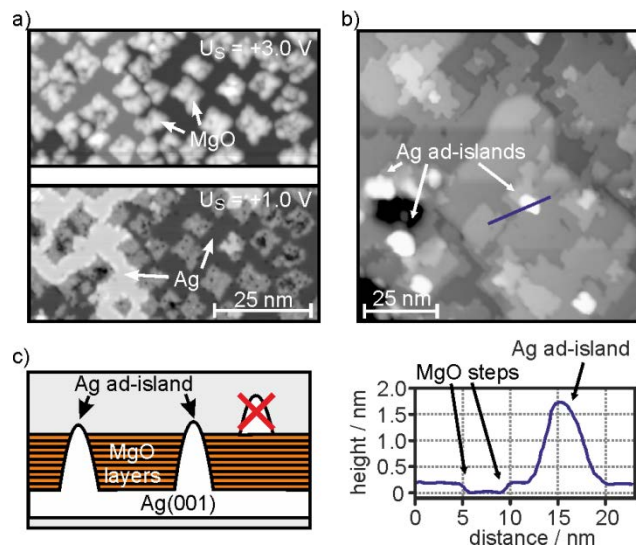


Figure 5. a) Low-temperature (5 K) STM micrographs (75 nm × 35 nm) of MgO monolayer-islands grown on Ag(001). The two images display the same area of the sample. The top image was recorded at a sample bias of $U_s = +3.0$ V, and the bottom image was recorded at $U_s = +1.0$ V. b) Low-temperature (5 K) STM micrograph (100 nm × 100 nm, $U_s = 3.5$ V) of a 4 ML MgO(001)/Ag(001) sample. Large bright spots in the image are identified as Ag islands. The height profile of one of the islands is shown below the STM image. c) Model showing that Ag ad-islands nucleate on the Ag(001) surface rather than on the surface of the MgO thin-film.

The STM results of Figure 5a are essentially identical to those reported by Schintke and Schneider and in agreement with findings of Valeri et al. [41]. Schintke and Schneider further noted that rather large islands of several nanometers height were observed on all MgO(001)/Ag(001) samples [38]. This statement is corroborated by our own observations on thicker MgO(001)/Ag(001) films. Figure 5b presents an STM image of a 4 ML MgO(001)/Ag(001) film showing flat, rectangular-shaped MgO(001) terraces and islands. In addition, a few bright features of several nanometers in diameter and up to 3 nm in height are seen in this image (as an example, we show the height profile of one of these features in the lower part of Figure 5b). Imaging at different bias voltages revealed that these features display no particular bias dependence, in contrast to the MgO-related structures. Therefore, they can be attributed to metallic Ag ad-islands, which are most likely formed during the early stages

of MgO growth when the first deposited monolayer of MgO is being completed. At this stage the individual MgO ad-islands grow in size and leave less space for diffusing Ag ad-atoms, which then agglomerate into larger islands and grow in height. This model suggests that the Ag ad-islands are in direct contact with the Ag(001) substrate instead of being nucleated on-top of the MgO thin film as supported nanoparticles (Figure 5c). Assuming that the islands are formed during the growth of the first one or two monolayers of MgO on Ag(001) and that they are stable throughout further growth, we estimate that an MgO amount equivalent to about 10-15 ML is required to completely cover the Ag ad-islands (the thickness of 1 ML MgO is 0.21 nm), in good agreement with the data presented in Section 3.3.

In order to corroborate the conclusions of the STM results we provide Figure 6, which shows synchrotron radiation excited Ag 3d photoemission spectra from Ag(001) and 15 ML MgO(001)/Ag(001), respectively. The spectra were taken at a photoelectron emission angle of 80° and a photoelectron kinetic energy of ~ 100 eV, i.e. at extreme surface sensitive conditions where the outermost 1-2 atomic layers of the surface are predominantly probed. The presence of a clear Ag 3d signal with a Ag 3d_{5/2} binding energy (BE) of 368.3 eV from 15 ML MgO(001)/Ag(001) points to the presence of Ag in the surface and near-surface region of this sample. From intensity analysis, the surface concentration of Ag on the MgO(001)/Ag(001) sample was calculated to be in the range of 0.3 – 3 atom-%, which is in reasonable agreement with the LEIS and $^{18}\text{O}_2$ -TPD data presented in Figure 4.

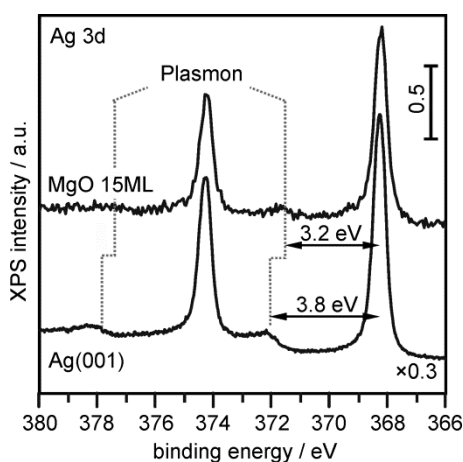


Figure 6. Synchrotron Ag 3d photoemission spectra of clean Ag(001) (bottom) and 15 ML MgO(001)/Ag(001) (top) recorded with a photon energy of 470 eV and a photoelectron emission angle of 80° with respect to the surface normal. Characteristic loss peaks due to plasmon excitation are indicated.

In addition, we note that characteristic loss features are observed for the two samples at $\Delta\text{BE} = 3.8$ eV for Ag(001) and at $\Delta\text{BE} = 3.2$ eV for MgO(001)/Ag(001). The 3.8 eV loss results from excitation of the well-known Ag surface plasmon characteristic for extended silver

surfaces as well as supported Ag nanoparticles, whereas the 3.2 eV loss is due to excitation of an MgO-Ag interface plasmon [42]. The absence of a surface plasmon loss peak in the case of the 15 ML MgO(001)/Ag(001) sample suggests that a large fraction of the Ag ad-islands' surface is in contact with MgO, rather than with vacuum (Figure 5c), which renders the presence of Ag particles nucleated and located on-top of the MgO surface unlikely. (Note that because of the small escape depth of the photoelectrons, we exclude that the observed plasmon loss peak originates from the interface between the extended Ag(001) substrate and the MgO overlayer.) We further note that the 3d core-level binding energies of Ag in the 15 ML MgO(001)/Ag(001) film and of Ag from the clean Ag(001) surface are identical. This observation suggests that Ag in MgO(001)/Ag(001) is in direct electrical contact with, rather than isolated from, the Ag(001) substrate. For isolated Ag ad-particles we would expect to observe a shift of the core-level binding energy to higher values relative to bulk Ag due to reduced screening of the core-hole in small particles.

Thus, our STM and XPS results corroborate the proposed model explaining the occurrence of Ag on thin MgO films by MgO growth-induced agglomeration of mobile Ag ad-atoms into islands of about 2-3 nm height. Neither STM nor XPS provides indications for the presence of individual, isolated Ag adatoms or small clusters embedded in the film or supported on the film surface. Therefore, local techniques such as STM will be well-suited for probing the properties of thin MgO(001)/Ag(001) films, as long as scanning in areas with Ag ad-islands is avoided. On the other hand, the results of studies using non-local techniques need to be treated with caution, since the presence of Ag or Ag-MgO interfaces may alter the reactivity of the thin-film sample (as shown here for CO oxidation), and give rise to additional, misleading spectral information.

One aspect that requires attention concerns the use of these films as model substrates for the growth of metal nanoparticles. To inform ourselves to what extent this is affected by the non-ideal MgO growth, we examined the nucleation of gold on thin MgO films as a function of film thickness. In Figure 7, we report IRA spectra taken from clean Ag(001) and various MgO(001)/Ag(001) samples following deposition of 0.04 ML Au and subsequent dosing with CO at 100 K. Since CO binds neither to Ag nor MgO at this temperature, the CO signals observed in the IRA spectra result exclusively from CO bound to Au. CO adsorption on Au deposited on the clean Ag(001) surface, which serves as a reference for the subsequent experiments with MgO(001)/Ag(001) films, gives rise to a single, sharp CO-IR band at 2098 cm^{-1} . The same band appears also in the IRA spectra recorded from the 1 ML and 2 ML

MgO(001)/Ag(001) films, along with bands at $\sim 2120\text{ cm}^{-1}$ and $\sim 2160\text{ cm}^{-1}$, which are attributed to CO adsorbed on MgO-supported Au clusters (see Ref. [43] for the assignment of these bands). For 3 ML MgO and thicker films, the band at 2098 cm^{-1} could not be observed, despite the presence of a significant fraction of exposed Ag on MgO(001)/Ag(001) films with a nominal MgO layer thickness of $< 10\text{ ML}$, as shown in the previous section. We conclude from this result that the exposed Ag spots are sufficiently small and widely separated on MgO films thicker than 2 ML MgO(001) such that at low deposition temperature, where diffusion lengths of Au ad-atoms are short, direct gold adsorption on, and diffusion of Au ad-atoms to exposed Ag is negligible. However, we do not exclude the possibility that at elevated temperatures, due to enhanced diffusion, some deposited metal particles would be able to diffuse to the exposed Ag areas and finally dissolve in the Ag(001) substrate.

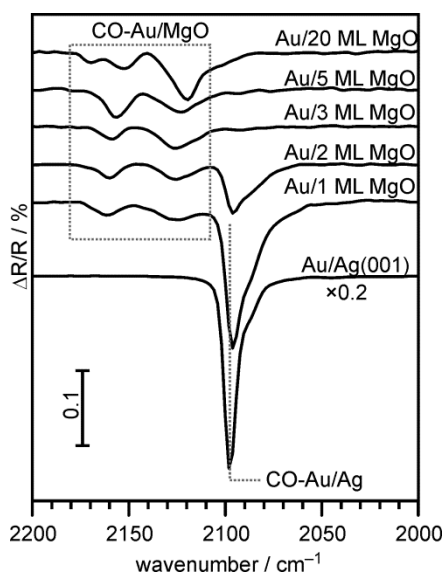


Figure 7. IRA spectra of CO adsorbed on 0.1 ML gold deposited on Ag(001) and MgO(001)/Ag(001) films of different MgO film thickness.

3.5 Catalytically active species in CO oxidation over MgO(001)/Ag(001) films

The results presented above suggest that exposed Ag is mainly responsible for the observed catalytic activity over MgO(001)/Ag(001) films under the CO oxidation conditions applied in this study. The non-covered lateral surface of the Ag single-crystal contributes a constant background activity to all samples, while exposed Ag ad-islands formed during MgO growth on Ag(001) are likely responsible for the enhanced CO oxidation activity of ultra-thin MgO(001)/Ag(001) films. The correlation between CO oxidation activity and the fraction of exposed Ag on samples of various MgO film thickness is presented in Figure 8. The Ag

surface concentration data were taken from the Ag-LEIS and $^{18}\text{O}_2$ -TPD results, Figure 4, and the CO oxidation activity data, taken from Figure 2b, is displayed as relative activity, which was calculated after subtraction of the constant background activity of the lateral crystal surface (grey-shaded area in Figure 2b) and using the activity of Ag(001) as reference. We note a positive deviation of the relative CO oxidation activity from that expected based on the area of exposed Ag. Since ultrathin MgO(001)/Mo(001) films were found to be completely inactive in CO oxidation (Figure 2c), we exclude that this deviation is the result of the intrinsic activity of ultrathin MgO(001)/Ag(001) films. Instead, we conclude that this effect is due to the enhanced specific activity of the Ag ad-islands formed during MgO film growth compared to that of the planar Ag(001) surface.

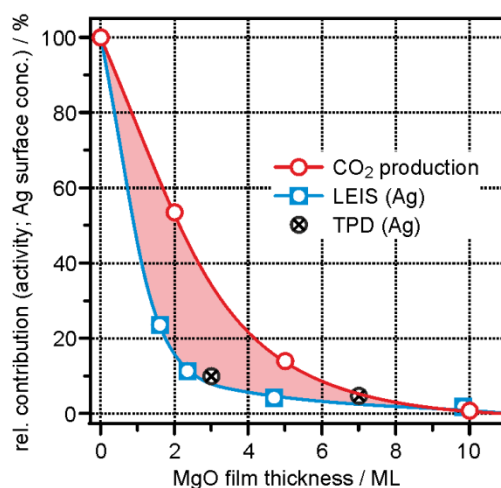


Figure 8. Correlation between MgO thickness dependent CO oxidation activity (red, relative to the CO oxidation activity of Ag(001) and after subtraction of the background activity of the non-covered later surface of the Ag(001) single-crystal sample) and the area of exposed Ag on thin MgO(001)/Ag(001) films (relative to Ag(001)) obtained from LEIS (blue) and $^{18}\text{O}_2$ -TPD (black) experiments. The shaded area indicates that the specific activity of Ag ad-islands formed during MgO growth is higher than that of the Ag(001) surface.

4 Conclusion

In this study we have shown that no promotional catalytic effect is found for ultra-thin MgO films grown on Ag(001) and Mo(001) in CO oxidation carried out under ambient-pressure reaction conditions. The enhancement of CO oxidation activity on ultra-thin MgO(001)/Ag(001) can readily be explained by the catalytic activity of Ag, which remains exposed on these samples. Detailed investigations of the growth and surface structure of MgO(001)/Ag(001) films suggest that Ag ad-islands are formed on the Ag(001) surface

during the initial stage of MgO growth. The Ag ad-islands are about 2-3 nm in height and the deposited amount of MgO required for their complete covering must exceed 15 ML.

We want to point out that the lack of intrinsic activity of thin MgO films in CO oxidation under elevated pressure conditions does not disprove previous theoretical and (mainly UHV) experimental studies that provided evidence for the occurrence of charge transfer through ultra-thin MgO films required for the activation of molecular oxygen on the MgO thin film surfaces, but might to some extent be associated with surface poisoning under the elevated-pressure reaction conditions employed in the present study. Indeed, we found a strong interaction of ultra-thin MgO(001)/Ag(001) films with the reaction gases (CO, O₂, residual water), resulting in surface functionalization by carbonates and hydroxyls. While poisoning of the surface is most likely responsible for the lack of intrinsic activity of supported MgO thin-films in CO oxidation, it also is a manifestation of the enhanced chemical activity of ultra-thin MgO(001) films compared to bulk-like MgO.

Acknowledgment

This work was supported by the Excellence initiative “UNICAT” sponsored by Deutsche Forschungsgemeinschaft and administered by TU Berlin. Y.F is grateful to DAAD and Co. Ltd. Takata for a fellowship. M.A.B, W.E.K. and F.C. thank the Alexander von Humboldt foundation for financial support. We thank Helmholtz-Zentrum Berlin for provision of synchrotron radiation.

References

- [1] H.-J. Freund, D.W. Goodman, Ultrathin Oxide Films, Handbook of Heterogeneous Catalysis, Wiley-VCH Verlag GmbH & Co. KGaA, 2008, pp. 1309-1338.
- [2] A.K. Santra, D.W. Goodman, J. Phys.: Condens. Matter 15 (2003) R31-R62.
- [3] H.-J. Freund, G. Pacchioni, Chem. Soc. Rev. 37 (2008) 2224-2242.
- [4] S.M. McClure, D.W. Goodman, Top. Catal. 54 (2011) 349-362.
- [5] J. Schoiswohl, S. Surnev, F.P. Netzer, Top. Catal. 36 (2005) 91-105.
- [6] J.A. Rodriguez, J. Hrbek, Surf. Sci. 604 (2010) 241-244.
- [7] S.D. Senanayake, D. Stacchiola, J.A. Rodriguez, Acc. Chem. Res. 46 (2013) 1702-1711.
- [8] G. Pacchioni, Chem. Eur. J. 18 (2012) 10144-10158.
- [9] H.-J. Freund, Surf. Sci. 601 (2007) 1438-1442.
- [10] M.-C. Wu, J.S. Corneille, J.-W. He, C.A. Estrada, D.W. Goodman, J. Vac. Sci. Technol. A 10 (1992) 1467-1471.
- [11] J. Wollschläger, D. Erdös, K.-M. Schröder, Surf. Sci. 402 (1998) 272-276.
- [12] S. Altieri, L.H. Tjeng, G.A. Sawatzky, Phys. Rev. B 61 (2000) 16948-16955.
- [13] L. Savio, E. Celasco, L. Vattuone, M. Rocca, J. Chem. Phys. 119 (2003) 12053-12056.
- [14] S. Schintke, S. Messerli, M. Pivetta, F. Patthey, L. Libioulle, M. Stengel, A. De Vita, W.-D. Schneider, Phys. Rev. Lett. 87 (2001) 276801.
- [15] G. Pacchioni, L. Giordano, M. Baistrocchi, Phys. Rev. Lett. 94 (2005) 226104.
- [16] D. Ricci, A. Bongiorno, G. Pacchioni, U. Landman, Phys. Rev. Lett. 97 (2006) 036106.
- [17] P. Frondelius, A. Hellman, K. Honkala, H. Häkkinen, H. Grönbeck, Phys. Rev. B 78 (2008) 085426.
- [18] M. Sterrer, T. Risse, U.M. Pozzoni, L. Giordano, M. Heyde, H.-P. Rust, G. Pacchioni, H.-J. Freund, Phys. Rev. Lett. 98 (2007) 096107.
- [19] M. Sterrer, T. Risse, M. Heyde, H.-P. Rust, H.-J. Freund, Phys. Rev. Lett. 98 (2007) 206103.
- [20] V. Simic-Milosevic, M. Heyde, X. Lin, T. König, H.-P. Rust, M. Sterrer, T. Risse, N. Nilius, H.-J. Freund, L. Giordano, G. Pacchioni, Phys. Rev. B 78 (2008) 235429.
- [21] X. Lin, N. Nilius, H.-J. Freund, M. Walter, P. Frondelius, K. Honkala, H. Häkkinen, Phys. Rev. Lett. 102 (2009) 206801.
- [22] X. Lin, N. Nilius, M. Sterrer, P. Koskinen, H. Häkkinen, H.-J. Freund, Phys. Rev. B 81 (2010) 153406.
- [23] C. Zhang, B. Yoon, U. Landman, J. Am. Chem. Soc. 129 (2007) 2228-2229.
- [24] A. Hellman, S. Klacar, H. Grönbeck, J. Am. Chem. Soc. 131 (2009) 16636-16637.
- [25] A. Gonchar, T. Risse, H.-J. Freund, L. Giordano, C. Di Valentin, G. Pacchioni, Angew. Chem. Int. Ed. 50 (2011) 2635-2638.
- [26] Y.-N. Sun, Z.-H. Qin, M. Lewandowski, E. Carrasco, M. Sterrer, S. Shaikhutdinov, H.-J. Freund, J. Catal. 266 (2009) 359-368.
- [27] Y.-N. Sun, L. Giordano, J. Goniakowski, M. Lewandowski, Z.-H. Qin, C. Noguera, S. Shaikhutdinov, G. Pacchioni, H.-J. Freund, Angew. Chem. Int. Ed. 49 (2010) 4418-4421.
- [28] Y. Martynova, S. Shaikhutdinov, H.-J. Freund, Chem. Cat. Chem. 5 (2013) 2162-2166.
- [29] T.C.R. Rocha, A. Oestereich, D.V. Demidov, M. Hävecker, S. Zafeiratos, G. Weinberg, V.I. Bukhtiyarov, A. Knop-Gericke, R. Schlögl, Phys. Chem. Chem. Phys. 14 (2012) 4554-4564.

- [30] M. Rocca, L. Savio, L. Vattuone, U. Burghaus, V. Palomba, N. Novelli, F.B. de Mongeot, U. Valbusa, R. Gunnella, G. Comelli, A. Baraldi, S. Lizzit, G. Paolucci, *Phys. Rev. B* 61 (2000) 213-227.
- [31] F. Werfel, E. Minni, *J. Phys. C: Solid State Phys.* 16 (1983) 6091-6100.
- [32] N.S. McIntyre, D.D. Johnston, L.L. Coatsworth, R.D. Davidson, J.R. Brown, *Surf. Interface Anal.* 15 (1990) 265-272.
- [33] Y. Iizuka, Y. Onishi, T. Tamura, T. Hamamura, *J. Catal.* 64 (1980) 437-447.
- [34] Y. Iizuka, M. Sanada, J. Tsunetoshi, J. Furukawa, A. Kumao, S. Arai, K. Tomishige, Y. Iwasawa, *J. Chem. Soc. Faraday Trans.* 92 (1996) 1249-1256.
- [35] S. Altieri, L.H. Tjeng, F.C. Voogt, A. Hibma, G.A. Sawatzky, *Phys. Rev. B* 59 (1999) R2517-R2520.
- [36] E.L. Garfunkel, X. Ding, G. Dong, S. Yang, X. Hou, X. Wang, *Surf. Sci.* 164 (1985) 511-525.
- [37] F.B. deMongeot, M. Rocca, A. Cupolillo, U. Valbusa, H.J. Kreuzer, S.H. Payne, *J. Chem. Phys.* 106 (1997) 711-718.
- [38] S. Schintke, W.D. Schneider, *J. Phys.: Condens. Matter* 16 (2004) R49-R81.
- [39] A. Ouvrard, J. Niebauer, A. Ghargaoui, C. Barth, C.R. Henry, B. Bourguignon, *J. Phys. Chem. C* 115 (2011) 8034-8041.
- [40] G. Cabailh, R. Lazzari, H. Cruguel, J. Jupille, L. Savio, M. Smerieri, A. Orzelli, L. Vattuone, M. Rocca, *J. Phys. Chem. A* 115 (2011) 7161-7168.
- [41] S. Valeri, S. Altieri, U. del Pennino, A. di Bona, P. Luches, A. Rota, *Phys. Rev. B* 65 (2002) 245410.
- [42] M.-H. Schaffner, F. Patthey, W.-D. Schneider, *Surf. Sci.* 417 (1998) 159-167.
- [43] M.A. Brown, F. Ringleb, Y. Fujimori, M. Sterrer, H.-J. Freund, G. Preda, G. Pacchioni, *J. Phys. Chem. C* 115 (2011) 10114-10124.